RSC Advances

PAPER

View Article Online
View Journal | View Issue

Cite this: *RSC Adv.*, 2026, **16**, 12238

NMR spectroscopic and computational analysis of *E*/*Z* isomerism in imines derived from isatin

Andrés Gonzalez-Oñate, [a] Diego Chaparro,[a] Rodolfo Quevedo, [a] Jorge Alí-Torres *[a] and Areli Flores-Gaspar *[b]

Received 24th December 2025
Accepted 26th February 2026

DOI: 10.1039/d5ra09983h

rsc.li/rsc-advances

Isatin reacts with primary amines to yield mixtures of *E* and *Z* imine stereoisomers. This study provides a detailed structural analysis of selected isatin-derived imines using ^{1}H and ^{13}C NMR spectroscopy, complemented by computational methods. The *E*/*Z* ratio in solution is shown to depend strongly on stabilization by solvent interactions and substituents attached to the imine nitrogen. Predominant isomer structures are typically stabilized by π-stacking between aromatic rings, highlighting the key role of non-covalent interactions in determining stereochemical products.

Introduction

Isatin is a benzo-fused cyclic ketone featuring a highly electrophilic carbonyl group, which enables its application in synthesizing diverse heterocyclic and spiroheterocyclic frameworks. These systems are widely recognized for their extensive biological activities.[1–5] In recent years, interest in isatin imines (Schiff bases) has grown compared to other derivatives; their structure, synthesis, and complexes have been studied for their potential biological and catalytic applications.[6–9]

Isatin derivatives, including imines, hydrazones, and semicarbazones, can adopt two stereoisomeric forms (*E* and *Z*) due to the restricted rotation around the C=N double bond.[8–12] The *E*/*Z* stereoisomerism in isatin hydrazones and semicarbazones has been attributed to the formation of intramolecular hydrogen bonds (Schemes 1A and 1B).[11,12] Noncovalent interactions preferentially stabilize one isomer, enabling their distinction by UV-Vis or NMR spectroscopy.

In isatin imines, intermolecular hydrogen bonding does not occur; however, both *E*- and *Z*-stereoisomers are still observed (Scheme 1c).[8–10] Previous studies have suggested that these stereoisomers exist in equilibrium, with the *E*-isomer considered the kinetic product and the *Z*-isomer the thermodynamic product. Nevertheless, a detailed structural explanation for this phenomenon in isatin imines has not yet been fully established.[7,8] Building on our previous investigations into the reactivity and structural properties of isatin derivatives,[10,13] this study explores the influence of the solvent, ring substituents on isatin, and amine nitrogen substituents on the *E*/*Z* isomerism and structure of isatin imines, using computational calculations and NMR spectroscopy.

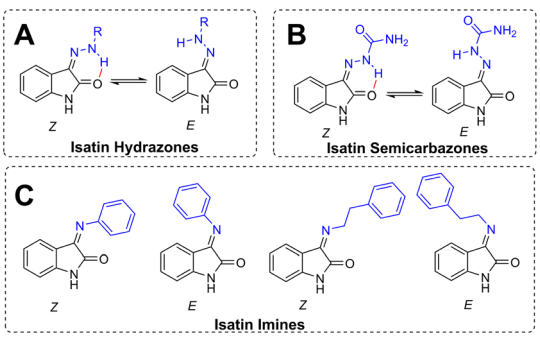

Scheme 1 Isomers of isatin hydrazones (A), semicarbazones (B), and imines (C).

Materials and methods

General

Commercially available solvents and reagents were used for the reactions in this work. Thin-layer chromatography (TLC) was used to monitor the reactions on silica gel-coated glass plates (Merck Kieselgel 60). The TLC plates were visualized by iodine vapor staining and UV detection. A Mel-Temp digital melting point electrothermal 9100 apparatus was used to determine melting points using open capillaries; reported values are uncorrected. Nuclear magnetic resonance (NMR) spectra were recorded at 26 °C (299 K) on a Bruker Avance NMR spectrometer, and chemical shifts (δ) are reported in parts per million (ppm) to the residual solvent peak. All NMR spectra were recorded 24 h after dissolving the sample to achieve equilibrium (Fig. S4). VTU calibration was made with standard method using methanol-d_4 (the difference between the chemical shift of –OH and –CH_3). For proportion estimation an standard Bruker

[a]*Departamento de Química, Universidad Nacional de Colombia, Sede Bogotá, Av. Cra. 30 No. 45-03, Bogotá, Colombia. E-mail: jialit@unal.edu.co*

[b]*Departamento de Química, Universidad Militar Nueva Granada, Cajicá 250240, Colombia. E-mail: areli.flores@unimilitar.edu.co*

zg30 pulse sequence were used. A Chromolith RP-18e monolithic column (Merck, Kenilworth, NJ, 50 mm) was used for UPLC analysis, using an Agilent 1200 Liquid Chromatograph (Agilent, Omaha, NE). The products were analyzed on a Bruker Impact II LC Q-TOF MS, equipped with electrospray ionization (ESI) in positive mode.

Computational details

Geometrical optimizations and frequency calculations in the gas phase were carried out using Gaussian 16 with the B3LYP DFT functional, Grimme's D3BJ dispersion correction, and the 6-311++G (d,p) basis set.[14–18] This combination of functional and basis sets has been proven to provide a proper geometrical and energy description, including long-range contributions with low computational cost.[19,20] To include solvent effects, the SMD solvation model was employed through single-point energy calculations on the optimized gas-phase geometries.[21–23]

Synthesis of isatin imines

Equimolar amounts of isatin (**1a–c**) were added to an amine (**2a–b**) solution (500 mg, 4 mmol) in methanol (10 mL). The mixture was stirred at room temperature (RT) for 24 hours. The precipitate was filtered and washed with cold methanol. The resulting product was characterized by melting point and ^{1}H- and ^{13}C-NMR spectroscopy (Scheme 2).

3-[(2-Phenylethyl)imino]-1,3-dihydro-2*H*-indol-2-one (**3a**) ($C_{16}H_{14}N_2O$). Yellow solid, yield: 77.4%, m.p. 134–136 °C. *E*-isomer (*E*-**3a**): ^{1}H-NMR (400 MHz, $CDCl_3$): δ 3,32 (2H,t,J = 7.7 Hz), 4.28 (2H,t,J = 7.7 Hz), 6.97 (1H,d,J = 7.8 Hz), 7.02 (1H,t,J = 7.6 Hz), 7.33–7.29 (5H,m), 7.36 (1H,t,J = 7.6 Hz), 7.61 (1H,d,J = 7.5 Hz), 9.75 (N–H). *Z*-isomer (*Z*-**3a**): ^{1}H-NMR (400 MHz, $CDCl_3$): δ 3.12 (2H,t,J = 7.7 Hz), 4.64 (2H,t,J = 7.7 Hz), 6.84 (1H,d,J = 7.8 Hz), 7.06 (1H,t,J = 7.6 Hz), 7.33–7.29 (overlapped), 7.36 (overlapped), 7.62(overlapped) 8.70 (N–H) (Fig. S1). ^{13}C-NMR *E*-isomer and *Z*-isomer (100 MHz, $CDCl_3$): δ 37.4, 37.7, 54.0, 56.3, 110.6, 111.9, 117.3, 122.4, 123.1, 126.2, 126.5, 127.1, 128.4, 128.7, 128.9, 129.1, 132.8, 133.7, 139.7, 140.0, 145.1, 155.0, 161.3, 165.7, 182.5, 184.9 (Fig. S2). *E*-isomer (*E*-**3a**): ^{1}H-NMR (400 MHz, d_6-DMSO): δ 3.15 (2H,t,J = 7.3 Hz), 4.22 (2H,t,J = 7.3 Hz), 6.90 (1H,d,J = 7.8 Hz), 7.23–7.17 (1H,m), 7.44–7.25 (overlapped), 7.69 (1H,d,J = 7.1 Hz), 10.88 (N–H). *Z*-isomer (*Z*-**3a**): ^{1}H-NMR (400 MHz, d_6-DMSO): δ 3.01(2H,t,J = 7.6 Hz), 4.52 (2H,t,J = 7.6 Hz), 6.85 (1H,d,J = 7.7 Hz), 7.05–6.98 (1H,m), 7.44–7.25 (overlapped), 7.47 (1H,d,J = 7.2 Hz), 10.81 (N–H) (Fig. S3). ^{13}C-NMR *E*-isomer and *Z*-isomer (100 MHz, d_6-DMSO): δ 36.7, 37.1, 52.8, 54.9, 110.5, 111.0, 116.6, 121.5, 121.6, 122.1, 122.2, 126.0, 126.1, 127.1, 128.2, 128.3, 128.7, 128.8, 132.9, 133.4, 140.0, 144.4, 145.8, 153.8, 154.7, 159.6, 163.6 (Fig. S5). ESI-MS (*m*/*z*): $[M + H]^+$ = 251.1196 (Calc. 251.1179) (Fig. S7).

5-Chloro-3-[(2-phenylethyl)imino]-1,3-dihydro-2*H*-indol-2-one (**3b**) ($C_{16}H_{13}N_2OCl$). Yellow solid, yield: 93.0%, m.p. 170–172 °C. *E*-isomer (*E*-**3b**): ^{1}H-NMR (400 MHz, d_6-DMSO): δ 3.15 (2H,t,J = 7.3 Hz), 4.22 (2H,t,J = 7.3 Hz), 6.90 (1H,d,J = 7.8 Hz), 7.23–7.17 (1H,m), 7.44–7.25 (overlapped), 7.69 (1H,d,J = 7.1 Hz), 10.88 (N–H). *Z*-isomer (*Z*-**3b**): ^{1}H-NMR (400 MHz, d_6-DMSO): δ 3.01(2H,t,J = 7.6 Hz), 4.52 (2H,t,J = 7.6 Hz), 6.85 (1H,d,J = 7.7 Hz), 7.05–6.98 (1H,m), 7.44–7.25 (overlapped), 7.47 (1H,d,J = 7.2 Hz), 10.81 (N–H) (Fig. S8). ^{13}C-NMR *E*-isomer and *Z*-isomer (100 MHz, d_6-DMSO): δ 36.9, 53.0, 112.2, 117.6, 121.1, 123.0, 123.9, 125.9, 126.0, 126.4, 128.2, 128.2, 128.4, 128.8, 128.9, 129.4, 139.9, 143.1, 153.0, 153.7, 159.2, 163.3 (Fig. S9). ESI-MS (*m*/*z*): $[M + H]^+$ = Not found (Calc. 285.0789). Precursors were found **1b** $[M + H]^+$ = 182.0001 (Calc. 182.0003), **2a** $[M + H]^+$ = 122.0964 (Calc. 122.0964) (Fig. S10).

5-Nitro-3-[(2-phenylethyl)imino]-1,3-dihydro-2*H*-indol-2-one (**3c**) ($C_{16}H_{13}N_3O_3$). Yellow solid, yield: 95.4%, m.p. 150 °C decomp. *E*-isomer (*E*-**3c**): ^{1}H-NMR (400 MHz, d_6-DMSO): δ 3.04 (2H,t,J = 7.6 Hz), 4.54 (2H,t,J = 7.6 Hz), 7.06 (1H,d,J = 8.8 Hz), 7.38–7.15 (overlapped), 8.9 (1H,dd,J = 8.8,2.5 Hz), 8.38 (1H,d,J = 2.5), 11.56 (N–H). *Z*-isomer (*Z*-**3c**): ^{1}H-NMR (400 MHz, d_6-DMSO): δ 3.17 (2H,t,J = 7.1 Hz), 4.33 (2H,t,J = 7.2 Hz), 7.03 (1H,d,J = 8.8 Hz), 7.38–7.15 (overlapped), 8.13 (1H,d,J = 2.5 Hz), 8.30 (1H,dd,J = 8.8,2.5 Hz), 11.56 (N–H). Phenylethylamine (**2a**): ^{1}H-NMR (400 MHz, d_6-DMSO): δ 2.28 (2H,t,J = 7.0 Hz), 3.50 (2H,t,J = 7.0 Hz), 7.38–7.15 (overlapped). 5-Nitroisatin (**1c**): ^{1}H-NMR (400 MHz, d_6-DMSO): 6.93 (1H,d,J = 9.0 Hz), 8.34–8.30 (overlapped), 8.61 (1H,d,J = 2.8 Hz) (Fig. S11)·^{13}C-NMR *E*-isomer, *Z*-isomer, phenylethylamine and 5-nitroisatin (100 MHz, d_6-DMSO): δ 34.7, 36.5, 36.9, 53.4, 55.2, 110.8, 111.0, 111.3, 116.1, 116.6, 117.6, 121.9, 122.4, 126.1, 128.3, 128.4, 128.3, 128.7, 128.8, 129.0, 129.0, 129.7, 131.1, 135.0, 139.0, 139.8, 142.0, 142.6, 149.8, 151.4, 152.3, 152.9, 156.5, 159.6, 163.7, 164.7, 191.0 (Fig. S12). ESI-MS (*m*/*z*): $[M + H]^+$ = Not found (Calc. 296.1030). Precursor was found **2a** $[M + H]^+$ = 122.0965 (Calc. 122.0964) (Fig. S13).

3-[(*p*-Methoxyphenyl)imino]-1,3-dihydro-2*H*-indol-2-one (**4a**) ($C_{15}H_{12}N_2O_2$). Orange solid, yield: 90.8%, m.p. 234–236 °C. *E*-isomer (*E*-**4a**): ^{1}H-NMR (400 MHz, d_6-DMSO): δ 3.80 (3H,s), 6.65 (1H,d,J = 7.8 Hz), 6.76 (1H,t,J = 7.7 Hz), 6.89 (1H,d,J = 7.8 Hz), 6.98 (2H,d,J = 9.0 Hz), 7.04 (2H,d,J = 9.0 Hz), 7.34 (1H,t,J = 7.7 Hz), 10.94 (N–H). *Z*-isomer (*Z*-**4a**): ^{1}H-NMR (400 MHz, d_6-DMSO): δ 3.77 (3H,s), 6.84 (1H,d,J = 7.7 Hz), 7.18 (2H,d,J = 8.9 Hz), 7.41 (1H,t,J = 7.7 Hz), 7.55 (1H,t,J = 7.6 Hz), 10.94 (N–H) (Fig. S14). ^{13}C-NMR *E*-isomer and *Z*-isomer (100 MHz, d_6-DMSO): δ 55.2, 55.3, 111.4, 113.4, 114.7, 115.8, 119.5, 121.7, 122.2, 122.8, 125.0, 134.2, 141.1, 143.1, 145.0, 146.8, 154.5, 157.1, 157.6, 163.6, 184.5 (Fig. S15). ESI-MS (*m*/*z*): $[M + H]^+$ = 253.0974 (Calc. 253.0972) (Fig. S16).

5-Chloro-3-[(*p*-methoxyphenyl)imino]-1,3-dihydro-2*H*-indol-2-one (**4b**) ($C_{15}H_{11}N_2O_2Cl$). Orange solid, yield: 72.7%, m.p. 216 °C decomp. *E*-isomer (*E*-**4b**): ^{1}H-NMR (400 MHz, d_6-DMSO): δ 3.81 (3H,s), 6.92 (1H,d,J = 8.4 Hz), 7.02 (1H,d,J = 9.0 Hz), 7.07 (1H,d,J = 9.0 Hz), 7.55 (1H,d,J = 2.3 Hz), 7.61 (1H,dd,J = 8.4,2.3 Hz), 11.13 (N–H). *Z*-isomer (*Z*-**4b**): ^{1}H-NMR (400 MHz, d_6-

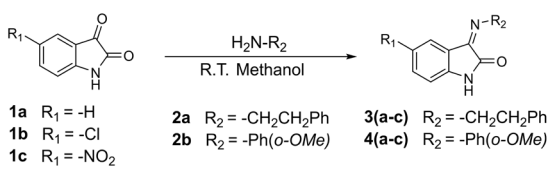

Scheme 2 General reaction procedure for isatin imine synthesis.

DMSO): δ 3.79 (3H,s), 6.58 (1H,d,J = 2.3 Hz), 6.92 (1H,d,J = 8.4 Hz), 7.27 (2H,d,J = 8.8 Hz), 7.40 (1H,dd,J = 8.4,2.3 Hz), 11.09 (N–H) (Fig. S17). ^{13}C-NMR *E*-isomer and *Z*-isomer (100 MHz, d_6-DMSO): δ 55.3, 55.4, 113.1, 113.4, 113.8, 114.8, 117.0, 119.1, 119.6, 121.8, 123.6, 125.2, 126.3, 126.8, 133.5, 137.3, 140.5, 142.6, 143.6, 145.6, 149.2, 153.5, 157.5, 158.1, 158.5, 159.2, 163.4, 183.3 (Fig. S18). ESI-MS (m/z): $[M + H]^+$ = 287.0585 (Calc. 287.0582) (Fig. S19).

5-Nitro-3-[(*p*-methoxyphenyl)imino]-1,3-dihydro-2*H*-indol-2-one (**4c**) ($C_{15}H_{11}N_3O_4$). Orange solid, yield: 88.6%, m.p. 233–235 °C. *E*-isomer (*E*-**4c**): ^{1}H-NMR (400 MHz, d_6-DMSO): δ 3.83 (3H,s), 7.06–7.12 (overlapped), 7.56 (1H,d,J = 2.3 Hz), 8.26 (1H,dd,J = 8.8,2.3 Hz), 11.65 (N–H). *Z*-isomer (*Z*-**4c**): ^{1}H-NMR (400 MHz, d_6-DMSO): δ 3.80 (3H,s), 6.95 (2H,d,J = 8.9 Hz), 7.04 (1H,d,J = 8.5 Hz), 7.40 (2H,t,J = 8.9 Hz), 8.33 (1H,dd,J = 8.5,2.3 Hz), 11.54 (N–H) (Fig. S20). ^{13}C-NMR *E*-isomer and *Z*-isomer (100 MHz, d_6-DMSO): δ 55.4, 55.5, 111.7, 113.5, 114.9, 115.7, 117.1, 112.0, 120.1, 123.0, 124.4, 129.1, 129.9, 140.0, 141.5, 142.2, 142.5, 149.2, 150.0, 152.1, 152.5, 157.9, 158.7, 159.1, 164.0 (Fig. S21). ESI-MS (m/z): $[M + H]^+$ = 298.0822 (Calc. 298.0822) (Fig. S22).

Results and discussion

Computational results

Previous reports have shown that the reaction between phenylethylamine and isatin yields a mixture of stereoisomers (Scheme 3). The *E* isomer forms as the kinetic product, while the *Z*-isomer corresponds to the thermodynamic product.[10] Isomerization of imine isomers proceeds *via* a planar inversion mechanism that involves a transition state (TS) with a specific geometry around imine nitrogen (Scheme 4).[24–26] To assess solvent effects on isomerization, the free energy of isomerization (ΔG^{gp}_{Isom}) and the free energy barrier ($\Delta G^{\neq}_{gp}$) in the gas phase were calculated using eqn (1) and (2).

$$\Delta G^{gp}_{Isom E\rightarrow Z} = G^{gp}_{Z\text{-isomer}} - G^{gp}_{E\text{-isomer}} \quad (1)$$

$$\Delta G^{\neq}_{gp E\rightarrow TS} = G^{gp}_{TS} - G^{gp}_{E\text{-isomer}} \quad (2)$$

To include solvent effects, we calculated the free energy of isomerization (ΔG^{sol}_{Isom}) and the free energy barrier ($\Delta G^{\neq}_{sol}$) in DMSO and chloroform (Fig. 1). These solvents were selected due to the solubility of the imines studied. These parameters were determined using eqn (3) and (4):

$$\Delta G^{sol}_{Isom E\rightarrow Z} = \Delta G^{gp}_{Isom E\rightarrow Z} - \Delta G^{solv}_{E\text{-isomer}} + \Delta G^{solv}_{Z\text{-isomer}} + \Delta nRT\ \ln(24.46) \quad (3)$$

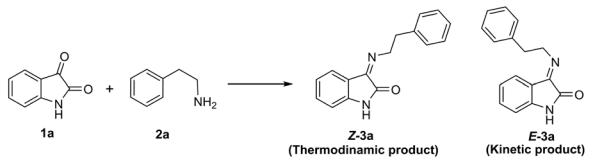

Scheme 3 Reaction products between phenylethylamine and isatin.

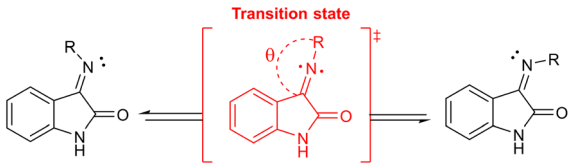

Scheme 4 Planar inversion isomerization mechanism of isatin imines with theta (θ) angle close to 180°.

$$\Delta G^{\neq}_{solE\rightarrow TS} = \Delta G^{\neq}_{gpE\rightarrow TS} - \Delta G^{solv}_{E\text{-isomer}} + \Delta G^{solv}_{TS} + \Delta nRT\ \ln(24.46) \quad (4)$$

Where, $\Delta G^{solv}_{E\text{-isomer}}$, $\Delta G^{solv}_{Z\text{-isomer}}$ and ΔG^{solv}_{TS} are the free energies of solvation, and the last term in both equations is the entropy correction from the concentration in the gas phase, assuming ideal gas conditions and a concentration of 1 M in solution.[22] For isomerization reactions, the change in the number of species at 298.15 K (Δn) is 0.

According to Fig. 2, solvation effects are crucial for the isomerization of isatin imines. In the gas phase and non-polar solvents, isomerization of *E*- to *Z*- isomer is spontaneous, whereas in polar solvents, the equilibrium shifts toward the *E*-isomer. The ΔG_{Isom} values are comparable to typical non-covalent interaction energies, indicating that both isomers coexist at equilibrium with similar concentrations. The *E*-isomer is stabilized in polar solvents because the nitrogen and oxygen atoms are more accessible for solvent interactions, which reduces the possibility of aromatic π-stacking between phenylethylamine and isatin. Conversely, the *Z*-isomer is favored in non-polar solvents, as its structure enables intramolecular π-stacking between aromatic rings. Consequently, a higher proportion of the *E*-isomer is expected in polar solvents, while the *Z*-isomer predominates in non-polar environments.

Optimized structures were correlated with NMR spectra to predict the predominant isomer in solution; positive $\Delta G^{sol}_{isomE-Z}$ values indicate a higher proportion of *E*-isomer, while negative values signal a greater proportion of *Z*-isomer. This prediction

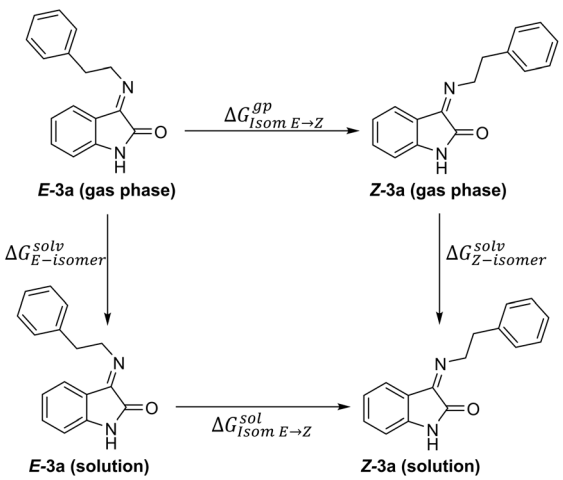

Fig. 1 Thermodynamic cycle used for the calculation of $\Delta G^{sol}_{Isom\ E\rightarrow Z}$.

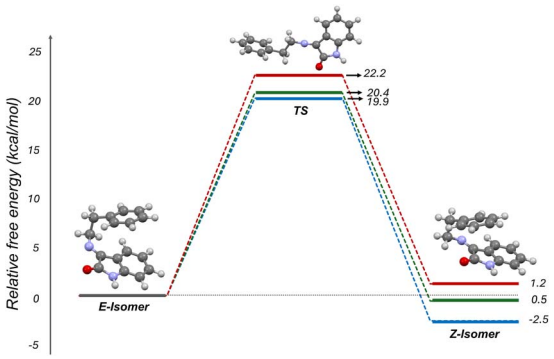

Fig. 2 Reaction profile for isomerization process ($E \rightarrow Z$) of **3a** in the gas phase (blue), chloroform (green), and DMSO (red).

aligns with Fig. 2, where integrals of each isomer's NMR signals reflect similar concentrations. Solvation effects impart only a minor influence on transition state stability, yet the activation energy barrier tends to increase with solvent polarity.

Effect of solvent on NMR spectra

Phenylethylamine was chosen for ^{1}H-NMR identification of *E*- and *Z*-isomers because its aliphatic protons yield signals in spectral regions free from overlap with other resonances. Both optimized isomer structures (Fig. 3) display a gauche conformation in the aliphatic chain, which likely arises from weak π-stacking interactions between the phenylethylamine aromatic ring and isatin.

To assign signals to each isomer, ^{1}H-NMR and NOESY spectra were recorded in DMSO-d6. An NOE correlation was expected only for the *E*-isomer; this correlation was observed between the aromatic proton *ortho* to the imino group of isatin at 7.69 ppm and the protons on the aliphatic carbon adjacent to the nitrogen at 4.22 ppm (Fig. 3A). COSY signals facilitated the assignment of signals at 3.15 and 4.22 ppm to the *E*-isomer and at 3.01 and 4.52 ppm to the *Z*-isomer (Fig. 4A).

The chemical shift difference between the aliphatic protons of each isomer is about 0.30 ppm, mainly due to their distinct geometries. The carbonyl group's anisotropy unshields protons in its plane, while those above or below are shielded. In the *Z*-isomer, the aliphatic chain's proximity to the carbonyl protects the methylene adjacent to the aromatic ring and deshields the

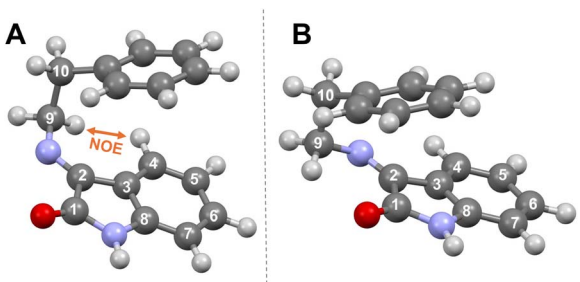

Fig. 3 Optimized structure of *E*-**3a** (A) and *Z*-**3a** (B) isomers.

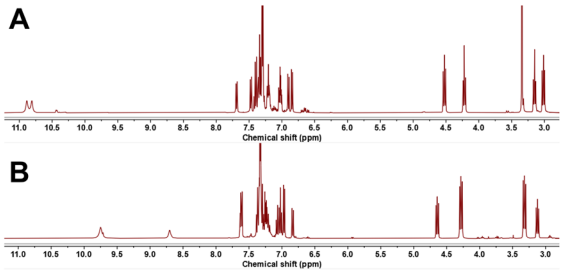

Fig. 4 ^{1}H-NMR of **3a** in DMSO (A) and chloroform (B).

methylene next to nitrogen, an effect absent in the *E*-isomer (see Fig. 3).[27,28]

EXSY spectra does not show any exchange peaks, however variable time NMR spectra of **3a** show the isomerization process occur and is too slow to present exchange peaks (Fig. S4). The equilibrium is archived approximately 24 h after dissolving the compound. (Fig. S23–S25).

To evaluate the effect of the solvent on chemical shift, ^{1}H-NMR spectra were also recorded in chloroform ($CDCl_3$) (Fig. 4B). All aliphatic signals showed a shift toward a lower field compared to the DMSO-d_6 spectra (Table 1), a trend attributed to shielding by the S=O bond anisotropy in DMSO, as aliphatic protons are close to the solvent's interaction sites with imine heteroatoms.[29]

The aromatic region (6.70–7.70 ppm) shows numerous signals, reflecting pronounced solvent effects on chemical shifts. In DMSO, doublets at 7.69 and 7.47 ppm correspond to the aromatic proton *ortho* to the imino group in the *E*- and *Z*-isomers, respectively. In chloroform, these signals overlap as a multiplet at 7.62 ppm. In contrast, the protons at 6.90 and 6.85 ppm in DMSO showed a greater difference in chloroform (6.97 and 6.84 ppm). These findings point out that solvent–solute interactions and anisotropic solvent effects play a key role in shielding or deshielding proton environments (Table 1).[29]

Amide (N–H) protons appear downfield in DMSO at 10.88 ppm (*E*-isomer) and 10.81 ppm (*Z*-isomer), with the *Z*-isomer showing additional shielding from the phenylethylamine aromatic ring. In $CDCl_3$, N–H signals shift upfield to 9.75 ppm (*E*) and 8.70 ppm (*Z*), with greater separation between

Table 1 Chemical shifts of relevant protons in **3a** isomers in chloroform ($CHCl_3$) and DMSO

Proton signal	$\delta(CHCl_3)$	δ(DMSO)	$\Delta\delta$(DMSO–$CHCl_3$)
N–H (*E*)	9.75	10.88	1.13
N–H (*Z*)	8.70	10.81	2.11
C4–H (*E*)	7.62	7.69	0.07
C4–H (*Z*)	7.62	7.47	−0.15
C7–H (*E*)	6.97	6.90	−0.07
C7–H (*Z*)	6.84	6.85	0.01
C9–H (*Z*)	4.64	4.52	−0.12
C9–H (*E*)	4.28	4.22	−0.06
C10–H (*E*)	3.32	3.15	−0.17
C10–H (*Z*)	3.12	3.01	−0.11

isomers. Hydrogen bonding between DMSO (acceptor) and N–H (donor) diminishes proton shielding and reduces chemical shift differences, an interaction absent in chloroform (Table 1 and Fig. 4).[29,30]

Imine substituent effect

Previous reports have shown that the reaction between anilines and isatin yields mixed stereoisomers, with the *E*-isomer being the major product (Scheme 5). To analyze the effect of the nitrogen substituent on the formation of the *E*- and *Z*-isomers, isatin imines were synthesized with *p*-anisidine and phenylethylamine, and their structures were optimized. The *p*-anisidine was used because the *p*-substituted ring simplifies the NMR spectra in the aromatic region and generates an aliphatic signal that allows differentiation of each isomer. Benzylamine was also reacted with isatin, resulting in a complex mixture that was analyzed.[31] All NMR spectra were recorded in DMSO due to solubility.

The ^{1}H-NMR spectrum of the imine derived from isatin and *p*-anisidine (**4a**) also showed the formation of the *E*- and *Z*-isomers (Fig. 5A). The methoxyl signals were observed at very close chemical shifts (3.80 and 3.77 ppm for *E*- and *Z*-, respectively). The aromatic proton signals appear between 6.60 and 7.60 ppm. The isatin aromatic proton near the imino group appears at 6.65 ppm for the *E*-isomer and at 6.84 ppm for the *Z*-isomer, while protons meta to the methoxy group are observed at 7.04 and 7.18 ppm. Greater anisotropic effects are detected in *E*-**4a** than in *Z*-**4a**, linked to the closer proximity of the *p*-substituted ring to the isatin moiety (Fig. 5B and C). Due to the isomer's geometry, anisotropic effects do not influence the isatin N–H proton, resulting in a single signal at 10.90 ppm for both isomers.

Computational calculations addressing *E*/*Z* isomerism in isatin-derived imines were carried out in DMSO, matching the solvent used for NMR measurements. Consequently, only the *E* to *Z* isomerization was considered since it is an exergonic process in DMSO. To evaluate the effect of the imine substituent on the isomerization, the free energy of isomerization ($\Delta G^{\mathrm{DMSO}}_{\mathrm{Isom}Z\rightarrow E}$) and the free energy barrier ($\Delta G^{\neq}_{\mathrm{sol}Z\rightarrow \mathrm{TS}}$) were calculated, as explained before in eqn (3) and (4).

As shown in Fig. 6, the substituents on the imine nitrogen greatly affect isomerization. Imine **4a** exhibits lower $\Delta G^{\neq}$ values and is more exergonic $\Delta G^{\mathrm{DMSO}}_{\mathrm{Isom}Z\rightarrow E}$ than imine **3a**, reflecting distinctive molecular geometries. In imine **3a**, π-stacking interactions stabilized both isomers (*Z*-**3a** and *E*-**3a**), resulting in a small energy gap between isomers. In contrast, imine **4a** lacks equivalent stabilization for both isomers; the *Z*-**4a** structure avoids the formation of non-covalent interactions to improve

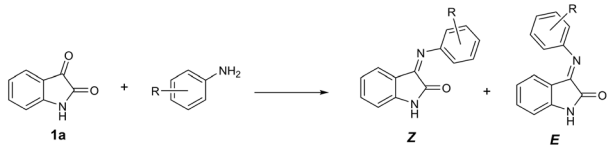

Scheme 5 Reaction products between anilines and isatin.

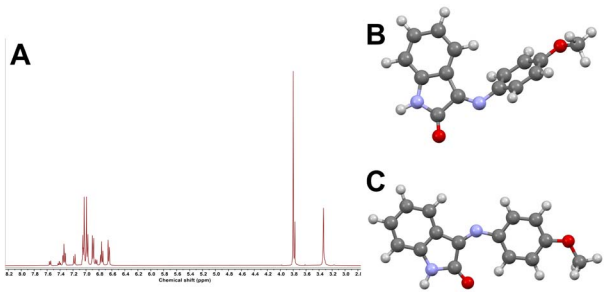

Fig. 5 ^{1}H-NMR of **4a** in DMSO (A), optimized structure of *E*-isomer (B) and *Z*-isomer (C).

steric hindrance, and *E*-**4a** can form non-covalent interactions between aromatic subunits. Those differences cause the energy difference between the two isomers to be higher than imine **3a**. Furthermore, reaching TS molecule **3a** requires breaking stabilizing π-stacking interactions and reorganizing its structure (conformers), which implies a higher energy cost and slow isomerization. For **4a**, weaker and more easily disrupted non-covalent interactions and minimal geometric rearrangement lower the energy barrier to isomerization.

To correlate the calculated $\Delta G^{\mathrm{DMSO}}_{\mathrm{Isom}Z\rightarrow E}$ with the NMR spectra, the isomerization constant in DMSO ($K^{\mathrm{DMSO}}_{\mathrm{Isom}Z\rightarrow E}$) was determined using the following equation:

$$K^{\mathrm{DMSO}}_{\mathrm{Isom}\ Z\rightarrow E} = e^{\frac{-\Delta G^{\mathrm{DMSO}}_{\mathrm{Isom}\ Z\rightarrow E}}{RT}} \quad (5)$$

NMR isomer ratios estimation were also determined using the integrals of aliphatic signals for equivalent protons in each isomer. Lower $K^{\mathrm{DMSO}}_{\mathrm{Isom}Z\rightarrow E}$ values correspond to a greater proportion of *Z*-isomer in solution.

As shown in Table 2, increasing $K^{\mathrm{DMSO}}_{\mathrm{Isom}Z\rightarrow E}$ raises the solution proportion of the *E*-isomer. This behavior was observed in NMR spectra, where **3a** has similar proportions of both isomers, in contrast to **4a**, where the *E*-isomer predominates. Phenylethyl groups stabilize both isomers through π-stacking, yielding nearly equal populations, whereas *p*-methoxyphenyl

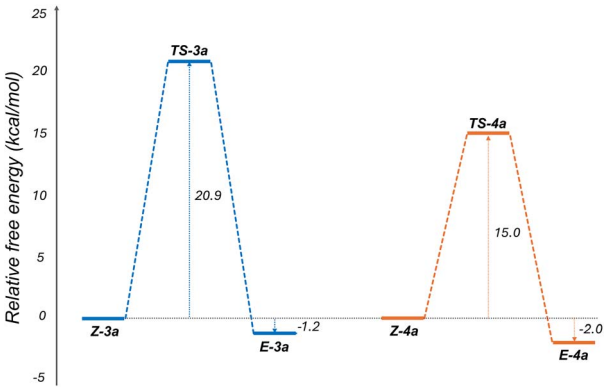

Fig. 6 Reaction profile for the isomerization (*Z* → *E*) in DMSO for **3a** (blue) and **4a** (orange) molecules.

Table 2 Thermodynamic parameters and NMR isomer proportion estimation for isatin imines[a]

Imine	$\Delta G^{DMSO}_{IsomZ\rightarrow E}$(kcal mol^{-1})	$K^{DMSO}_{IsomZ\rightarrow E}$	NMR isomer proportion estimation ($E:Z$)
3a (–H)	−1.2	7.7	47 : 53
3b (–Cl)	−1.5	13.2	56 : 44
3c (–NO_2)	−1.6	14.5	37 : 63
4a (–H)	−2.0	29.9	80 : 20
4b (–Cl)	−1.7	18.7	75 : 25
4c (–NO_2)	−1.5	13.1	71 : 29

[a] Proportion estimation was calculated with the integral of aliphatic proton signals.

substitution preferentially stabilizes the *E*-isomer and increases its proportion.

Isatin substituent effect

To evaluate the effect of isatin substituents, isomerization analyses were also performed for 5-chloroisatin (**1b**) and 5-nitroisatin (**1c**). NMR isomer ratios were determined using the integration of methoxy proton signals, and for **4a–c** and **3a–c**, by the methylene signals adjacent to the phenylethylamine aromatic ring.

According to Table 2, the effect of isatin substituents on isomerization depends on the imine's nitrogen substituent. For the *N*-phenylethyl substituent, an increase in electron-withdrawing effect caused by the substituent on the isatin ring slightly increases the proportion of the *E*-isomer. π-stacking interaction between the isatin aromatic ring and the phenylethylamine ring in the *E*-isomer is favored with electron-withdrawing groups. A high stabilizing effect of π-stacking interactions was achieved between electron-rich and electron-poor aromatic rings.[32,33] However, for imine **3c**, this trend is absent, likely due to partial hydrolysis in DMSO. For *N*-*p*-methoxyphenyl imines, electron-withdrawing groups favor the *Z*-isomer by destabilizing *E*-isomer noncovalent interactions. Overall, isatin substituents generally have only a minor impact on isomerization equilibria.

Conclusion

The *E*/*Z* isomer ratio in isatin imines is governed by the solvent and molecular substituents, which modulate structural stabilization through π-stacking interactions. In polar solvents, *E*-isomer formation is favored, largely independent of isatin or imine nitrogen substituents, as isatin substituents minimally affect isomerization. Substituents on the imine nitrogen, however, play a major role *via* non-covalent interactions. *N*-phenylethyl group enable π-stacking that equally stabilizes both isomers, resulting in similar ratios. In contrast, *N*-*p*-methoxyphenyl group form π-stacking that preferentially stabilizes the *E*-isomer, increasing its abundance in solution.

Author contributions

A. G-O: writing-original draft, formal analysis, investigation. D. C: investigation. R. Q: supervision, conceptualization, writing-review and editing. J. A-T: supervision, conceptualization, writing-review and editing. A. F-G: projet administration.

Conflicts of interest

There are no conflicts to declare.

Data availability

The data supporting this article have been included as part of the supplementary information (SI). Supplementary information: https://drive.google.com/file/d/1JjTEoCvABB9IcGXNOpPgdezjybKr1N9k/view?usp=sharing. See DOI: https://doi.org/10.1039/d5ra09983h.

Acknowledgements

A. G.-O. and J. A.-T. thank to DIEB-UNAL and the Center of Excellence in Scientific Computing (CoE-SciCo) for continuous support (Project 57465 – Universidad Nacional de Colombia). R. Q. thanks, Universidad Nacional de Colombia for financial support (Project 65584). A. F.-G. thanks, Universidad Militar Nueva Granada for financial support (Project INV CIAS 2535).

Notes and references

1 S. N. Pandeya, S. Smitha, M. Jyoti and S. K. Sridhar, Biological activities of isatin and its derivatives, *Acta Pharm*, 2005, **55**, 27–46.

2 M. C. Rodríuez-Argüelles, M. Belicchi Ferrari, F. Bisceglie, C. Pelizzi, G. Pelosi, S. Pinelli and M. Sassi, Synthesis, characterization and biological activity of Ni, Cu and Zn complexes of isatin hydrazones, *J. Inorg. Biochem.*, 2004, **98**, 313–321, DOI: 10.1016/j.jinorgbio.2003.10.006.

3 A. Bacchi, M. Carcelli, P. Pelagatti, G. Pelizzi, M. C. Rodriguez-Arguelles, D. Rogolino, C. Solinas and F. Zani, Antimicrobial and mutagenic properties of organotin(IV) complexes with isatin and N-alkylisatin bisthiocarbonohydrazones, *J. Inorg. Biochem.*, 2005, **99**, 397–408, DOI: 10.1016/j.jinorgbio.2004.10.008.

4 E. Labisbal, A. Sousa, A. Castiñeiras, J. A. García-Vázquez, J. Romero and D. X. West, Spectral and structural studies of metal complexes of isatin 3-hexamethyleneiminylthiosemicarbazone prepared

electrochemically, *Polyhedron*, 2000, **19**, 1255–1262, DOI: 10.1016/s0277-5387(00)00383-1.

5 Y. Kaya, A. Erçağ, Y. Zorlu, Y. Demir and İ. Gülçin, New Pd(II) complexes of the bisthiocarbohydrazones derived from isatin and disubstituted salicylaldehydes: Synthesis, characterization, crystal structures and inhibitory properties against some metabolic enzymes, *J. Biol. Inorg. Chem.*, 2022, **27**, 271–281, DOI: 10.1007/s00775-022-01932-9.

6 G. Cerchiaro, K. Aquilano, G. Filomeni, G. Rotilio, M. R. Ciriolo and A. M. D. C. Ferreira, Isatin-Schiff base copper(II) complexes and their influence on cellular viability, *J. Inorg. Biochem.*, 2005, **99**, 1433–1440, DOI: 10.1016/j.jinorgbio.2005.03.013.

7 A. S. Smirnov, L. M. D. Martins, D. N. Nikolaev, R. A. Manzhos, V. V. Gurzhiy, A. G. Krivenko, K. O. Nikolaenko, A. V. Belyakov, A. V. Garabadzhiu and P. B. Davidovich, Structure and catalytic properties of novel copper isatin Schiff base complexes, *New J. Chem.*, 2019, **43**, 188–198, DOI: 10.1039/c8nj02718h.

8 P. Davidovich, D. Novikova, V. Tribulovich, S. Smirnov, V. Gurzhiy, G. Melino and A. Garabadzhiu, First X-ray structural characterization of isatin Schiff base derivative. NMR and theoretical conformational studies, *J. Mol. Struct.*, 2014, **1075**, 450–455, DOI: 10.1016/j.molstruc.2014.07.008.

9 D. R. Brkić, A. R. Božić, A. D. Marinković, M. K. Milčić, N. Ž. Prlainović, F. H. Assaleh, I. N. Cvijetić, J. B. Nikolić and S. Ž. Drmanić, Detailed solvent, structural, quantum chemical study and antimicrobial activity of isatin Schiff base, *Spectrochim. Acta A Mol. Biomol. Spectrosc.*, 2018, **196**, 16–30, DOI: 10.1016/j.saa.2018.01.080.

10 Y. Vélez, C. Díaz-Oviedo and R. Quevedo, Kinetic and thermodynamic control in β-phenylethylamines reaction with isatin, *J. Mol. Struct.*, 2017, **1133**, 430–435, DOI: 10.1016/j.molstruc.2016.12.039.

11 K. Jakusová, M. Gáplovský, J. Donovalová, M. Cigáň, H. Stankovičová, R. Sokolík, J. Gašpar and A. Gáplovský, Effect of reactants' concentration on the ratio and yield of E,Z isomers of isatin-3-(4-phenyl)semicarbazone and N-methylisatin-3-(4-phenyl)semicarbazone, *Chem. Pap.*, 2013, 67, DOI: 10.2478/s11696-012-0248-x.

12 M. Cigáň, K. Jakusová, M. Gáplovský, J. Filo, J. Donovalová and A. Gáplovský, Isatin phenylhydrazones: anion enhanced photochromic behaviour, *Photochem. Photobiol. Sci.*, 2015, **14**, 2064–2073, DOI: 10.1039/c5pp00275c.

13 M. Umba-Erazo and R. Quevedo, An oxidative expansion mechanism of isatin-derived imines, *J. Chem. Sci.*, 2024, **136**, 45, DOI: 10.1007/s12039-024-02283-5.

14 M. J. T. Frisch, G. W. Schlegel, H. B. Scuseria, G. E. Robb, M. A. Cheeseman, J. R. Scalmani, G. Barone, V. Petersson, G. A. Nakatsuji, H. Li, X. Caricato, M. Marenich, A. V. Bloino, J. Janesko, B. G. Gomperts, R. Mennucci, B. Hratchian, H. P. Ortiz, J. V. Izmaylov, A. F. Sonnenberg, J. L. Williams-Young, D. Ding, F. Lipparini, F. Egidi, F. Goings, J. Peng, B. Petrone, A. Henderson, T. Ranasinghe, D. Zakrzewski, V. G. Gao, J. Rega, N. Zheng, G. Liang, W. Hada, M. Ehara, M. Toyota, K. Fukuda, R. Hasegawa, J. Ishida, M. Nakajima, T. Honda, Y. Kitao, O. Nakai, H. Vreven, T. Throssell, K. Montgomery, J. A. Jr. Peralta, J. E. Ogliaro, F. Bearpark, M. J. Heyd, J. J. Brothers, E. N. Kudin, K. N. Staroverov, V. N. Keith, T. A. Kobayashi, R. Normand, J. Raghavachari, K. Rendell, A. P. Burant, J. C. Iyengar, S. S. Tomasi, J. Cossi, M. Millam, J. M. Klene, M. Adamo, C. Cammi, R. Ochterski, J. W. Martin, R. L. Morokuma, K. Farkas, O. Foresman J.B. and D. J. Fox *Gaussian 16, Revision C.01*, Gaussian, Inc., Wallingford CT, 2016.

15 A.-R. Allouche, Gabedit–a graphical user interface for computational chemistry softwares, *J. Comput. Chem.*, 2011, **32**, 174–182, DOI: 10.1002/jcc.21600.

16 A. D. Becke, Density-functional thermochemistry. I. The effect of the exchange-only gradient correction, *J. Chem. Phys.*, 1992, **96**, 2155–2160, DOI: 10.1063/1.462066.

17 C. Lee, W. Yang and R. G. Parr, Development of the Colle-Salvetti correlation-energy formula into a functional of the electron density, *Phys. Rev. B Condens. Matter*, 1988, **37**, 785–789, DOI: 10.1103/physrevb.37.785.

18 S. Grimme, S. Ehrlich and L. Goerigk, Effect of the damping function in dispersion corrected density functional theory, *J. Comput. Chem.*, 2011, **32**, 1456–1465, DOI: 10.1002/jcc.21759.

19 J. Alí-Torres, A. Rimola, C. Rodríguez-Rodríguez, L. Rodríguez-Santiago and M. Sodupe, Insights on the binding of Thioflavin derivative markers to amyloid-like fibril models from quantum chemical calculations, *J. Phys. Chem. B*, 2013, **117**, 6674–6680, DOI: 10.1021/jp402807g.

20 A. Gonzalez-Oñate, J. Alí-Torres and R. Quevedo, The role of non-covalent interactions in 4-hydroxybenzylamine macrocyclisation: computational and synthetic evidence, *RSC Adv.*, 2024, **14**, 3691–3697, DOI: 10.1039/d3ra08508b.

21 A. V. Marenich, C. J. Crame and D. G. Truhlar, Universal solvation model based on solute electron density and on a continuum model of the solvent defined by the bulk dielectric constant and atomic surface tensions, *J. Phys. Chem. B*, 2009, **113**, 6378–6396, DOI: 10.1021/jp810292n.

22 J. Alí-Torres, L. Rodríguez-Santiago and M. Sodupe, Computational calculations of pKa values of imidazole in Cu(II) complexes of biological relevance, *Phys. Chem. Chem. Phys.*, 2011, **13**, 7852–7861, DOI: 10.1039/c0cp02319a.

23 C. F. Macrae, I. Sovago, S. J. Cottrel, P. T. A. Galek, P. McCabe, E. Pidcock, M. Platings, G. P. Shields, J. S. Stevens, M. Towler and P. A. Wood, Mercury 4.0: from visualization to analysis, design and prediction, *J. Appl. Crystallogr.*, 2020, **53**, 226–235, DOI: 10.1107/S1600576719014092.

24 F. P. Cossío, A. de Cózar, M. A. Sierra, L. Casarrubios, J. G. Muntaner, B. K. Banik and D. Bandyopadhyay, Role of imine isomerization in the stereocontrol of the Staudinger reaction between ketenes and imines, *RSC Adv.*, 2021, **12**, 104–117, DOI: 10.1039/d1ra06114c.

25 A. B. Rozhenko, A. A. Kyrylchuk, Y. O. Lapinska, Y. V. Rassukana, V. V. Trachevsky, V. V. Pirozhenko, J. Leszczynski and P. P. Onysko, Z,E-isomerism in a series of substituted iminophosphonates: Quantum chemical

research, *Organics.*, 2021, **2**, 84–97, DOI: 10.3390/org2020008.

26 R. Knorr, J. Ruhdorfer, J. Mehlstäubl, P. Böhrer and D. S. Stephenson, (E, Z)1-equilibria, 17 demonstration of the nitrogen inversion mechanism of imines in a Schiff base model, *Chem. Ber.*, 1993, **126**, 747–754, DOI: 10.1002/cber.19931260327.

27 S. Kold and E. Kleinpeter, *Ab initio* calculation of the anisotropy effect of multiple bonds and the ring current effect of arenes—application in conformational and configurational analysis, *J. Chem. Soc. Perkin Trans 2*, 2001, (10), 1893–1898, DOI: 10.1039/B009809O.

28 O. Staszewska-Krajewska, W. Bocian, M. Maciejko, P. Szcześniak, K. Szymczak, M. Chmielewski and B. Furman, The use of carbonyl group anisotropy effect in determination of the relative configuration of carbapenams, *ARKIVOC.*, 2014, **3**, 143, DOI: 10.3998/ark.5550190.p008.450.

29 R. J. Abraham, J. J. Byrne, L. Griffiths and M. Perez, 1H chemical shifts in NMR: Part 23, the effect of dimethyl sulphoxide *versus* chloroform solvent on 1H chemical shifts, *Magn. Reson. Chem.*, 2006, **44**, 491–509, DOI: 10.1002/mrc.1747.

30 S. Molchanov and A. Gryff-Keller, Solvation of amides in DMSO and CDCl3: An attempt at quantitative DFT-based interpretation of 1H and 13C NMR chemical shifts, *J. Phys. Chem. A*, 2017, **121**, 9645–9653, DOI: 10.1021/acs.jpca.7b10110.

31 W. G. Brouwer, W. A. Craig, J. A. D. Jeffreys and A. Munro, The reaction between isatin and some amines, *J. Chem. Soc., Perkin Trans.*, 1972, **1**, 124–129, DOI: 10.1039/p19720000124.

32 C. R. Martinez and B. L. Iverson, Rethinking the term "pi-stacking", *Chem. Sci.*, 2012, **3**, 2191, DOI: 10.1039/c2sc20045g.

33 K. Carter-Fenk and J. M. Herbert, Reinterpreting π-stacking, *Phys. Chem. Chem. Phys.*, 2020, **22**, 24870–24886, DOI: 10.1039/d0cp05039c.